

Method to extract multiple states in F₁-ATPase rotation experiments from jump distributions

Sándor Volkán-Kacsó^{a,b,1}, Luan Q. Le^c, Kaicheng Zhu^d, Haibin Su^{d,1}, and Rudolph A. Marcus^{a,1}

a Noyes Laboratory of Chemical Physics, California Institute of Technology, Pasadena, CA 91125; Department of Mathematics, Physics and Statistics, Azusa Pacific University, Azusa, CA 91702; School of Materials Science and Engineering, Nanyang Technological University, Singapore 639798; and Department of Chemistry, Hong Kong University of Science and Technology, Clear Water Bay, Hong Kong

Contributed by Rudolph A. Marcus, October 23, 2019 (sent for review September 4, 2019; reviewed by Hiroyuki Noji and Attila Szabo)

A method is proposed for analyzing fast (10 µs) single-molecule rotation trajectories in F₁ adenosinetriphosphatase (F₁-ATPase). This method is based on the distribution of jumps in the rotation angle that occur in the transitions during the steps between subsequent catalytic dwells. The method is complementary to the "stalling" technique devised by H. Noji et al. [Biophys. Rev. 9, 103-118, 2017], and can reveal multiple states not directly detectable as steps. A bimodal distribution of jumps is observed at certain angles, due to the system being in either of 2 states at the same rotation angle. In this method, a multistate theory is used that takes into account a viscoelastic fluctuation of the imaging probe. Using an established sequence of 3 specific states, a theoretical profile of angular jumps is predicted, without adjustable parameters, that agrees with experiment for most of the angular range. Agreement can be achieved at all angles by assuming a fourth state with an \sim 10 μ s lifetime and a dwell angle about 40° after the adenosine 5'-triphosphate (ATP) binding dwell. The latter result suggests that the ATP binding in one β subunit and the adenosine 5'-diphosphate (ADP) release from another β subunit occur via a transient whose lifetime is \sim 10 μs and is about 6 orders of magnitude smaller than the lifetime for ADP release from a singly occupied F1-ATPase. An internal consistency test is given by comparing 2 independent ways of obtaining the relaxation time of the probe. They agree and are \sim 15 μ s.

F-ATPase | single-molecule imaging | concerted dynamics | 4-state model | ADP release

denosine 5'-triphosphate (ATP) synthase is known to con-Avert the energy in the proton gradient across the mitochondrial membrane into chemical energy needed to synthesize ATP (1). Proton transport in the membrane-bound F_O adenosinetriphosphatase (F_O-ATPase) ring produces a rotation of an asymmetric γ shaft in the F_1 -ATPase part. The rotation, in turn, causes conformational changes in the asymmetric catalytic subunits, ultimately leading to ATP synthesis (2). The F₁-ATPase studied in single-molecule experiments functions as a rotary motor. It produces a rotation of the γ shaft relative to its barrel-like $\alpha_3\beta_3$ stator structure, and is powered by the hydrolysis of ATP (3). The chemistry and rotation in F_1 -ATPase are the reverse of that in ATP synthase, and the study of rotation in the former can reveal the rotary mechanism in the latter (4).

The rotation in the thermophylic bacillus F₁-ATPase shown in Fig. 1A is produced in steps of 120° (5) that can be resolved into substeps of 80° and 40° at low ATP concentration (6). During its rotation cycle, the F₁-ATPase motor proceeds through a series of transitions from one biochemical state to another. These transitions lead to a time evolution of a mechanical rotation coordinate monitored in single-molecule imaging experiments by attaching a probe to the γ shaft. As illustrated in Fig. 1B, the rotation angle "hovers" around specific dwell angles, and then it transitions from one dwell to the next one.

Beyond resolving the dwell angles between steps, high-speed microsecond time resolution imaging techniques using nanoscale probes, (9, 10) also capture data points during the transitions

(Fig. 1A). In this article, we treat these data, and address several

- 1) In the single-molecule stalling (11) and controlled rotation experiments (12), angle-dependent rate constants have been extracted for various substeps. It is assumed, in the analysis of stalling data, that, at a given rotation angle θ , obtained by magnetic tweezers, the system can jump between 2 states. We explore here whether a method can be devised to detect these multiple states at the same angle in fast (10 μs) free rotation trajectories, that is, without magnetic tweezers.
- 2) The smallest probes currently used in single-molecule experiments [40-nm gold bead (13)] still produce viscous friction during rotation. The rotor complex is elastically compliant and can twist under torque loads (14). Taking into account the viscoelastic response time τ involved in a convolution of the underlying biochemical states, we explore a methodology for extracting "hidden" states in the transitions.
- 3) The larger of the 2 rotation substeps, the 80° substep, is associated with the binding of ATP to an empty β subunit and the release of a product adenosine 5'-diphosphate (ADP) from the counterclockwise β , viewed from where the F_O-ATPase would be in a complete ATP synthase (7). These 2 events appear to be concerted at a millisecond time resolution, and we investigate whether an intermediate state might be revealed in the fast microsecond timescale experiments, involving a possibly concerted ATP binding-ADP release mechanism.

Significance

In single-molecule imaging of the F₁-ATPase rotation by nanoprobes, there are jumps in the angular position. Their distribution is used in a method for detecting hidden states in the transitions during rotation steps. Complementing stalling experiments, this method reveals, now in free rotation without magnetic tweezers, that the motor can be in either of 2 states at a rotation angle. A comparison between the experimental trajectories and a multistate theory reveals that an 80° substep of the coupled ATP binding and ADP release involves an intermediate state reminiscent of a 3-occupancy structure. Its lifetime (\sim 10 μ s) is comparable with the frame time of the imaging, so, by detecting this short-lived state, the method provides an increased effective time resolution.

Author contributions: S.V.-K., H.S., and R.A.M. designed research: S.V.-K., L.O.L., and K.Z. performed research; S.V.-K. and L.Q.L. analyzed data; and S.V.-K., L.Q.L., and R.A.M. wrote the paper.

Reviewers: H.N., University of Tokyo; and A.S., NIH.

The authors declare no competing interest.

Published under the PNAS license.

¹To whom correspondence may be addressed. Email: ram@caltech.edu, svk@caltech.edu, or haibinsu@ust.hk.

This article contains supporting information online at https://www.pnas.org/lookup/suppl/ doi:10.1073/pnas.1915314116/-/DCSupplemental.

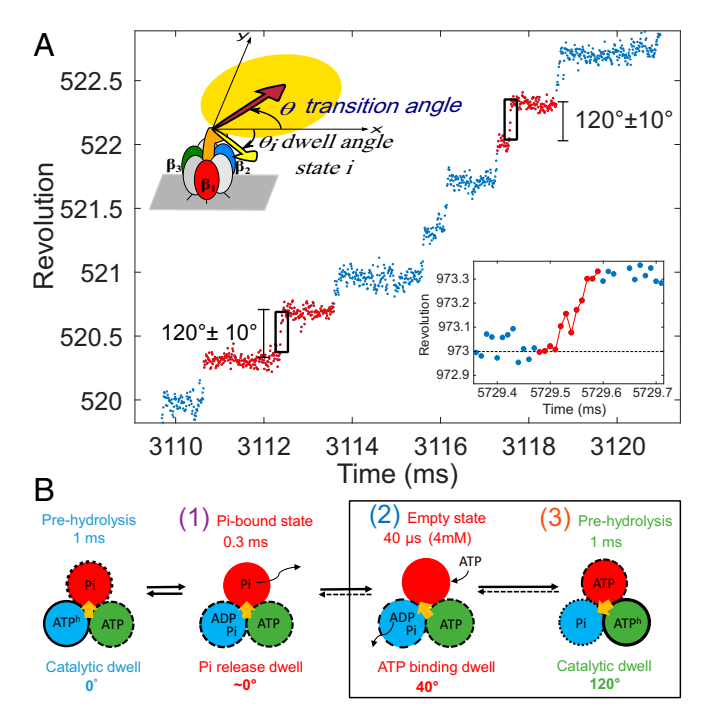


Fig. 1. (A) F1-ATPase single-molecule imaging trajectory showing stepping behavior: Longer dwells are separated by faster transitions. The latter, which are the focus of the present analysis, may show both upward and downward jumps (*Lower Right Inset*). The assay uses a gold nanocrystal as optical probe (*Upper Left Inset*). (B) The rotation coupling scheme resolved in previous experiments (3, 6–9) containing 3 chemical states and their lifetimes (including the ATP waiting state at 4 mM ATP concentration). Reactions occurring during transitions are boxed.

Mirroring these 3 topics, the structure of this article is organized around 3 main findings. First, a method for studying fast transitions is described in *Multistate Model for Rotation Jumps in the F*₁-ATPase Model, based on angular jump distribution and using a theory of multiple states. Using this method in *Application of the Theory to Free Rotation*, the presence of 2 states at the same θ angle in the trajectories is demonstrated, thus supporting the current interpretation of stalling experiments (11).

Second, agreement of a 3-state model with experiment is demonstrated in *Application of the Theory to Free Rotation*, for most of the angle range with no adjustable parameters. One of the states in the 3-state model involves a hidden ATP binding step.

Third, evidence for a ~ 10 -µs metastable state containing both ADP and ATP is postulated in *Application of the Theory to Free Rotation* to explain the data. The predictions are discussed in *Discussion*, and the mechanistic insights suggested by the present method are summarized in *Summary of Predictions and Insights*.

Multistate Model for Rotation Jumps in the F₁-ATPase Motor

We assume a series of steps described by a discrete occupancy state (or chemical state) variable i. As depicted in Fig. 1B, an experimentally detectable dwell angle θ_i corresponds to each state i, in particular the P_i release dwell (i=1), the ATP binding dwell (i=2), and the catalytic dwell (i=3). The transitions are rare but fast, so θ is quasi-static during any particular transition (15), and one can speak of rate constants $k(\theta)$. Our main assumption is that, at any θ , regardless of whether that θ is at a dwell or is an angle in between dwells, a reaction can occur with rate constant $k(\theta)$. We note the distinction between states i and the processes taking the systems from one state to another, for example, the empty (ATP waiting) state 2 and ATP binding

step $2 \rightarrow 3$. In the quasi-static approximation, then (15), $k_{fi}(\theta)$ and $k_{bi}(\theta)$ are the angle-dependent rate constants for the transitions between the states i and i+1, as described in a subsequent section.

The rotation angle θ in single-molecule imaging experiments is subject to Brownian fluctuations. The probe experiences viscous drag from the water molecules. It diffuses with a rotational diffusion constant D. Any contributions from the viscous load on the γ shaft and "internal friction" in the protein are included in D. The probe is also subject to an elastic (14) torque, $-\kappa_r(\theta-\theta_i)$, that pulls it toward the dwell angle θ_i in state i of the system. κ_r is the effective rotational (torsional) elastic constant for the bead-rotor-ring system (γ is presumably coupled to multiple α and β subunits). In state i, the viscoelastic relaxation time of the system (e.g., ref. 16) is

$$\tau = (D\beta \kappa_r)^{-1}.$$
 [1]

The angular probability density $\rho_i(\theta,t)$ of being in state i follows a diffusion–reaction equation, an approach pioneered by Oster and Wang (17), who considered a scheme of 64 possible states. Instead, in the present method, we use a specific sequence of several states with specific transfer rates between them, given later in Eqs. 4 and 5. The latter $k_{fi}(\theta)$ and $k_{bi}(\theta)$ act as "source" or "sink" terms for a given state,

$$\frac{\partial \rho_i}{\partial t} = D \frac{\partial}{\partial \theta} \left[\beta \kappa_r (\theta - \theta_i) \rho_i \right] + D \frac{\partial^2 \rho_i}{\partial \theta^2}
- \left[k_{f,i}(\theta) + k_{b,i-1}(\theta) \right] \rho_i + k_{f,i-1}(\theta) \rho_{i-1} + k_{b,i}(\theta) \rho_{i+1}.$$
[2]

The i dependence of D and κ_{τ} has been suppressed. We will assume that these quantities (and so τ) are identical for all states. In a more general case, different τ_i s may apply to states i. Assuming some initial and boundary conditions, and a particular number of states i, the system of Eq. 2 can be solved numerically.

Angular Dependence of the Jumps. To calculate the θ dependence of the jumps, besides the $\rho_i(\theta)$, the distribution of angular jumps $\rho_{ii}(\theta+\Delta\theta,t+\Delta t|\theta,t)$ is also introduced: It is a conditional probability distribution that the system survives in state i (there is no reaction) at time $t+\Delta t$ and is found at angle $\theta+\Delta\theta$, if, at time t it was at θ . In this analysis, Δt is the time step (frame time) of the imaging apparatus. A solution for the $\rho_{ii}(\theta+\Delta\theta,t+\Delta t|\theta,t)$ is found by inserting it into Eq. 2 with rate constant terms removed and using a delta function initial condition (cf. ref. 16 and *SI Appendix*). When Δt is small compared to the viscoelastic relaxation time τ , the approximate solution is a Gaussian with a θ -dependent peak that is independent of t. In a simplified notation, this solution is (see equations 4.55 and 5.32 in ref. 16)

$$\rho_{ii}(\Delta\theta \mid \theta) \cong \frac{1}{2\sqrt{\pi D\Delta t}} \exp\left\{-\frac{[\Delta\theta/\Delta t - (1/\tau)(\theta_i - \theta)]^2}{4D/\Delta t}\right\}.$$
[3]

The peak of the angular jump distribution occurs at $(\Delta\theta/\Delta t) = (\theta_i - \theta)/\tau$, and so the expectation value $\langle \Delta\theta/\Delta t \rangle$ is linear in θ with a slope of $-1/\tau$.

A key quantity used in the current analysis is the experimentally observed angular jump distribution of the system, defined as the probability of a jump at a set angle, $\rho(\Delta\theta/\Delta t\,|\,\theta)$. It is plotted, from experiments and calculations, in Fig. 2 A and B, respectively. Another important quantity is the average of the angular jumps at a certain rotor angle, $\langle \Delta\theta \rangle/\Delta t$, and it is plotted versus θ later in *Application of the Theory to Free Rotation*. They are calculated by solving Eq. 2 for probability $\rho_i(\theta,t)$, then summing over all components in Eq. 3, as described in detail in *Materials and Methods*.

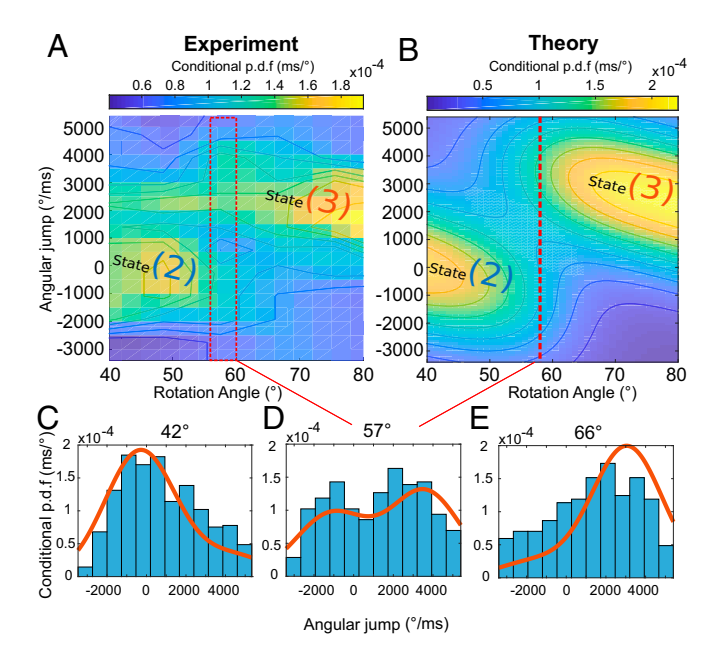


Fig. 2. (A) Experimental angular jump distribution and (B) its theoretical counterpart in an angular range of 40° to 80° where bimodal behavior can be detected. (C–E) Experimental (bars) and theoretical (red curves) jump distributions at 3 angles in the region of overlap of states 2 and 3. Two peaks of similar height are resolved in D at rotor angles indicated by the red dashed lines in A and B. p.d.f., probability distribution function.

Angle-Dependent Rate Constants. When the system is at the reactant's free energy minimum, θ fluctuates around the dwell $\theta_{r,i} = \theta_i$; after a fast transition, during which θ is quasi-static, the system is in the product state, and it relaxes toward, and fluctuates about, the product dwell $\theta_{p,i} = \theta_{i+1}$. We note that the θ_r s and θ_f s correspond to the initial and final angles for a transfer reaction (θ_i and θ_f) in equation 4 of ref. 18. The fluctuations of θ in the dwells are significant, with an SD of $\sim 20^\circ$ (Fig. 1A and SI Appendix, Fig. S1). In the elastic transfer model, the forward and back rate constants $k_f(\theta)$ and $k_{bi}(\theta)$ are predicted to be exponential functions (18) over a limited θ range probed in the stalling experiments (7, 11),

$$k_{fi}(\theta) = k_{fi}(\theta_i) \exp[a_{fi}(\theta - \theta_i)],$$
 [4]

$$k_{bi}(\theta) = k_{bi}(\theta_i) \exp[-a_{bi}(\theta - \theta_i)],$$
 [5]

where k_{bi} is the rate constant for reactions from state i+1 back to state i. The angular coefficients are $a_{fi}=\beta\alpha_i\kappa_{ci}s_i$ and $a_{bi}=\beta(1-\alpha_i)\kappa_{ci}s_i$ (18), where $s_i=(\theta_{i+1}-\theta_i)$ is the step size, $\beta=1/k_BT$, and the spring constant κ_c describes the coupling between the mechanical rotation and a reaction progress coordinate. α_i is the Brønsted slope used in previous work (18). In this work, coefficients a_{fi} and a_{bi} from stalling experiments are used for the ATP binding (see *Materials and Methods*).

Application of the Theory to Free Rotation

Bimodal Distribution of Angular Jumps. We consider the transitions (average duration $\sim 120~\mu s$ corresponding to 12 time steps) between subsequent catalytic dwells (average duration $\sim 1~ms$ per dwell) in the trajectories whose step size falls within $120^{\circ}\pm 10^{\circ}$ (SI Appendix). Individual angular jumps are defined as angular displacements $\Delta\theta=\theta'-\theta$ from one time frame to the next in the rotation trajectories. The distributions of jumps divided with Δt and renormalized now with respect to $\Delta\theta/\Delta t$, $\rho(\Delta\theta/\Delta t\mid\theta)$, are plotted in Fig. 2A. They were extracted from the transitions using a method prompted by the work of Frasch and coworkers,

(10, 19), who use the "angular velocity" term for this normalized jump, $\Delta\theta/\Delta t$.

In this work, θ is defined relative to the catalytic dwells clearly resolved in the trajectories (Fig. 1A). These dwells occur at 0° , 120° , 240° , etc. (In another reference frame (3, 18), these dwells are at -40° , 80° , 200° , etc.) The experimental probability densities of jumps showed a single-peaked Gaussian distribution in a range of roughly 0° to 40° , termed hereafter as "region I," and in another range from 80° to 120° ("region III"). However, in the angular "region II" between 40° and 80° , a markedly different distribution of 2 distinctive peaks emerges and is seen as "mountain ranges" in Fig. 2A, with a "valley" in between. At around 60° , the 2 peaks have similar heights and yield the resolved bimodal distribution seen in Fig. 2D, as compared with Figs. 2A and C.

Multiple States at the Same Rotation Angle. The distribution of jumps was qualitatively reproduced by a 3-state model in Fig. 1B based on the established sequence of 3 consecutive events (3, 6-9, 20). In accord with earlier reports (6), we found that the distribution of waiting times in the catalytic dwells can be best fit with 2 exponentials (SI Appendix, Fig. S8), suggesting that both hydrolysis and Pi release occur during this dwell (6). Their lifetimes, according to the distribution of waiting times in the dwell (SI Appendix, Fig. S8), are \sim 1 ms and \sim 0.5 ms, respectively, which is consistent with previous reports (6). Then, the events occurring during transitions are the binding of ATP and the release of ADP, followed by the transition to the next catalytic dwell (Fig. 1B). At 4 mM concentration, the ATP binding dwell at 40° is too brief to be resolved by a simple inspection of the trajectories, but the empty (ATP waiting) state 2 is resolved here.

The 2 peaks in the distributions in Fig. 2A and B correspond to states i=2 and 3 in the transitions (in Fig. 1B, the "empty" and "prehydrolysis" states, respectively). In the multistate model, it is predicted that, around a certain angle ($\theta=57^{\circ}$), the system may be in either state 2 or 3 with similar probability, effectively giving rise to the bimodal distribution of angular jumps in Fig. 2A.

Average Angular Jump in the 3-State Model. For a more detailed quantitative analysis, the mean angular jump $\Delta\theta$ serves as a basis to compare theory and experiment. We found that the mean jump profile predicted by a 3-state model (Fig. 3A) agrees with the experimental data roughly in regions I and III on that figure, with no adjustable parameters. For this purpose, as described in *Materials and Methods*, independent data were taken from the dwells in the current trajectories and other experiments. As described in *Discussion*, there is an agreement between the previously defined τ extracted from the trajectories in 2 independent ways, namely, 1) from the average jump vs. θ slope in region III of the data found in the transition between dwells and 2) from the fluctuations in the dwell, at $\theta=0$ (SI Appendix, Fig. S7).

The signature of the ATP binding dwell is seen in the dip of the jump around 40° in Fig. 3A, as expected according to the active kinetic scheme (11). The prediction of the 3-state model deviates from the experimental jump profile roughly in the range of $50^\circ < \theta < 80^\circ$: The dashed line in Fig. 3A shows a high predicted peak at 70° which arises from a large angular step of 80° from the ATP waiting state to the precatalysis state. Using the observed turnover in the exponential rate constants (i.e., $k(\theta)$ increases with θt ; then, beyond a turnover angle it decreases; cf. figure 2 in ref. 21) in Eqs. 4 and 5, instead of the exponential form for k_{f2} in the turnover region, did not affect the theoretical results in Fig. 3A (SI Appendix, Fig. S11) significantly, for reasons given later in Discussion.

A Short-Lived State after ATP Binding and before ADP Release. Agreement between theory and experiment can be achieved in

Volkán-Kacsó et al. PNAS Latest Articles | 3 of 6



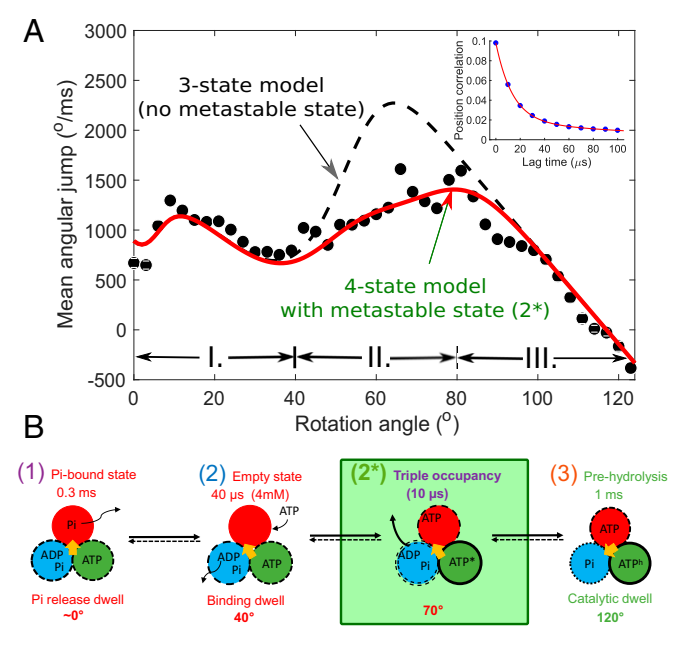


Fig. 3. (A) The mean of the angular jumps "normalized" by dividing with $\Delta\theta$. Experimental data (black circles) were compared with theoretical predictions from a 3-state model (black dashed line) using no adjustable parameters (Table 1) and a 4-state model (solid red line). The ranges for the 3 regions are designated at the bottom of the plot. (Inset) The θ autocorrelation function in the dwells, fitted to $\langle \theta(t+t_0)\theta(t_0)\rangle=0.08e^{-t/14}+0.02e^{-t/140}$; t in microseconds. (B) Reaction scheme in F₁-ATPase according to a 4-state model.

all regions on Fig. 3A, and, in particular, in the region of the high peak, if an intermediate state is postulated in the transition between the empty (ATP waiting) state 2 and the prehydrolysis state 3. It would be a short-lived fourth state, denoted by 2*, with a lifetime of 10 μ s and a dwell angle $\theta_{2*} = 76^{\circ} \pm 5^{\circ}$ (Table 1). A 4-state model (Fig. 3B), now with 2 adjustable parameters $(k_{f2^*}(\theta_{2^*}))$ and θ_{2^*} , yields the solid red line in Fig. 3A. For state 2^* , a Brønsted slope of $\alpha_{2^*} = 1/2$ was assumed in Fig. 3A, but we explored the limits of its possible values, 0 to 1 (SI Appendix, Fig. S13), and found that the specific time $1/k_{f2^*}(\theta_{2^*})$ for the state varies roughly between 10 µs and 13 µs. The values used for k_r and D were the same as the values in the other 3 states. In Fig. 3A, the θ -dependent mean jump shows distinct "sensitivity" to the presence or absence of the postulated $\theta_{2*} = 76^{\circ}$ state, even as its lifetime is comparable with the time resolution of $\Delta t = 10 \mu s$ of the apparatus. Using a kinetic model then, for the statistical treatment of experimental trajectories, in effect increases the temporal resolution (22, 23), which is analogous to previous methods used to extract fast protein folding rates from single-molecule fluorescence resonance energy transfer data (22, 24).

Discussion

Concerted Conformation and Kinetic Intermediate. In the F_1 -ATPase motor, the spontaneous release of ADP would be very slow on its own (~ 1 min), as seen in single-site occupancy experiments (3, 12). ADP release is accelerated by some 6 orders of magnitude when it is coupled with an ATP binding event in another β subunit, that is, under physiological ATP concentrations (millimolar range). The strong interaction between the subunits gives rise ultimately to unidirectional rotation (8, 20). At millisecond time resolution, the ATP binding and the ADP release appear to be a single concerted process. At higher time resolution, a short-lived kinetic intermediate is resolved ($i=2^*$) with a dwell at 36° after the ATP binding dwell.

For the intermediate, we postulated a state containing both the incoming ATP and outgoing ADP, similar to the state postulated by Walker et al. (25) in which all 3 β subunits are occupied by nucleotides. Alternatively, sequential kinetics for the ATP binding/ADP release was suggested (3, 26, 27), but a kinetic intermediate was previously undetected. Its ~10- μ s lifetime suggests a microsecond timescale for the lifetime of the proposed intermediate state. Its dwell at $\theta=76^{\circ}$ causes the average angular jumps in Fig. 3A to be smaller, thus explaining why the solid red line is below the dashed line.

These results may be compared to those of Chung et al. (28) in protein folding, where transitions between only 2 observed states were studied. In the 120° transitions in the F_1 -ATPase, there are more states. An alternative view for the 10- μ s state is that there is a barrier instead of a well as shown in Fig. 4, analogous to a theory for 2-state folding by Cossio et al. (29). However, we assume that the diffusion times to traverse an angle of, say, 5° at the top of the barrier, as distinct from the times to reach the top of the barrier, are much shorter than $10~\mu$ s. For example, a 10^4 degrees squared per microsecond angular diffusion constant yields a diffusion time of $\sim 1~\text{ns}$ (SI Appendix).

In experiments with magnetic tweezers by Saita et al. (30), a linear torque versus angle dependence was found to be interrupted by sawtooth-like transitions. We plan to investigate these features using the present theory, in particular, whether a torque transition 20° to 40° after ATP binding is related to fourth state postulated.

Table 1. Physical quantities in the 4-state model

State i	Substep	θ_i (deg)	$k_{fi}(\theta_i)$ (ms ⁻¹)	<i>a_i</i> (1/deg)	α_i	κ_r (pN nm)	$D(deg/\mu s)$	References, equations [†]
0, 3	Hydrolysis	0, 116	1	0.019	~1	72	12	Ref. 32 and the <i>SI Appendix</i> ; ref. 11; refs. 11 and 18 and Eq. 4; ref. 18; <i>SI Appendix</i> , Eq. 58; Eq. 1 and <i>SI Appendix</i> , Eq. 58
1	Pi release	~0	3	0.117	~0.7	72	12	Ref. 32 and the <i>Si Appendix</i> ; refs. 7 and 18, Eq. 4; refs. 7 and 18; ref. 18; <i>SI Appendix</i> , Eq. S8 ; Eq. 1 and <i>SI Appendix</i> , Eq. S8
2	ATP binding (4 mM)	36	40	0.045	0.5	72	12	Ref. 32; refs. 11 and 18, Eq. 4; refs. 11 and 18; ref. 18; <i>SI Appendix</i> , Eq. S8 ; Eq. 1 and <i>SI Appendix</i> , Eq. S8
2*	(ADP release)	76	80	0.045	0.5	72	12	Fig. 3; Fig. 3; ref. 12 and Eq. 4; refs. 12 and 18; SI Appendix, Eq. 58; Eq. 1 and SI Appendix, Eq. 58

[†]References and equations used to estimate the quantities in columns 3–8 are grouped in 6 groups in order according to the columns to which they refer. Groups are separated by semicolons, e.g., items before the first semicolon refer to column 3.

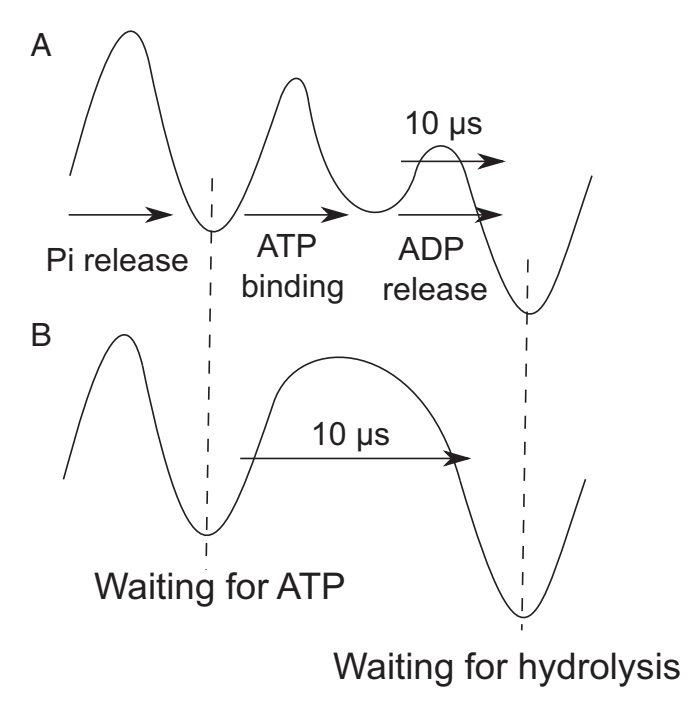


Fig. 4. (A) Series of substeps in the 120° transitions with the 10- μ s transient postulated in this work. (B) Alternative view for the 10- μ s transition following ref. 29.

Relaxation Time τ in the Dwell and in the Transition. In region III of the transition, between 100° and 120° , the system is found predominantly in the prehydrolysis state 3 and so the rotary probe would tend to relax toward the next catalytic dwell. According to Eq. 3, there should be a linear dependence of the average angular jump on θ in Fig. 3A. For small Δt , the slope of the $\langle \Delta \theta \rangle / \Delta t$ vs. θ function approximates the inverse of the viscoelastic relaxation time $1/\tau$ in this state 3. The slope of the linear part of $\langle \Delta \theta \rangle / \Delta t$ in region III in the experimental data is seen to yield about 20 µs for τ (Fig. 3A). Using instead the more general Eq. 6, at finite $\Delta t = 10$ µs, this slope corresponds instead to $\tau = 15$ µs. Meanwhile, in the current work, τ was also estimated independently in the catalytic dwell, using the correlation function, $\langle \theta(t_1)\theta(t_2)\rangle$. Its short-time exponential decay seen in Fig. 3A, Inset yielded a $\tau = 14$ µs, in good agreement with the 15 µs found in region III.

Effect of the Turnover in the Exponential Rate Constants. A "turnover" occurs at a certain θ when $k_{f2}(\theta)$ reaches a maximum, presumably due to the closing of a cleft in the β subunit (15). Using a turnover, the theory produced identical jump distributions to those without a turnover (SI Appendix, Fig. S11), since the system has reacted before reaching the turnover region (SI Appendix).

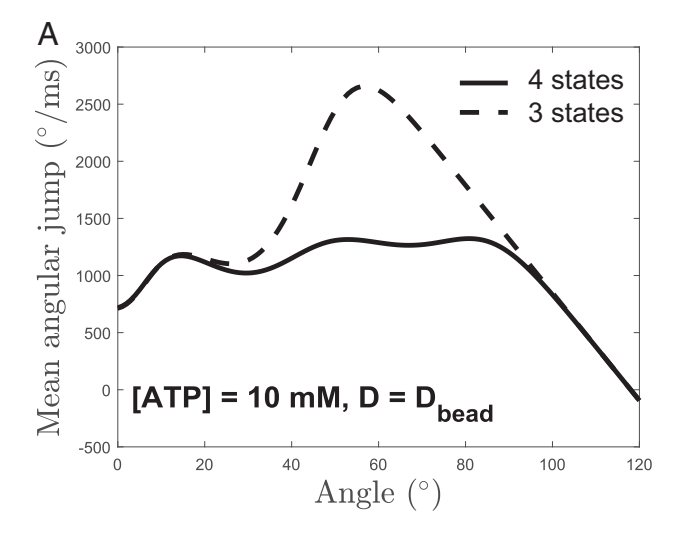
Mean Jump Profile at Different ATP Concentrations. At increased ATP concentration, a single large peak dominates on Fig. 5A. The resulting difference between a 3-state and a 4-state model is more dramatic than at lower ATP concentrations, and so can be used to further test the consequences of the prediction of the fourth state. The jump profile is sensitive to the lifetime of this state, as seen on the plots for 3, 10, and $30~\mu s$ on Fig. 5B.

Langevin Simulations. Langevin-type equations have been used to simulate F_1 -ATPase rotation (13) and protein folding (29). We plan to implement this approach for the present method to study the transitions in Fig. 4. Simulated trajectories can be subjected to the same method of analysis that is applied to experimental data.

Summary of Predictions and Insights

We conclude by listing the key predictions by the model.

- 1) Multiple states were detected at the same rotation angle in fast rotation experiments. The jump distribution from the free rotation trajectories was used in conjunction with theory to detect states in the transitions between dwells. A direct observation of dual peaks in the distributions at an angle supports an assumption made in the interpretation (7) of the stalling experiments. It is a key assumption needed to extract angledependent rate constants for the ATP binding, P_i release, and catalysis steps in these experiments (8, 11).
- 2) A metastable state is postulated, previously not detectable at slower time resolution. The average jump vs. rotation angle predicted for the 3-state model agrees with experiment over most of the angle range. It deviates from experiment in a range $50^{\circ} < \theta < 80^{\circ}$ (Fig. 3A), and, assuming harmonic rotation potentials in all states, agreement between theory and experiment is achieved by postulating a fourth state with a dwell angle at $\sim 36^{\circ}$ after the binding dwell. Increasing ATP concentration is predicted to result in an increased difference between the 3- and 4-state models. In the present method,



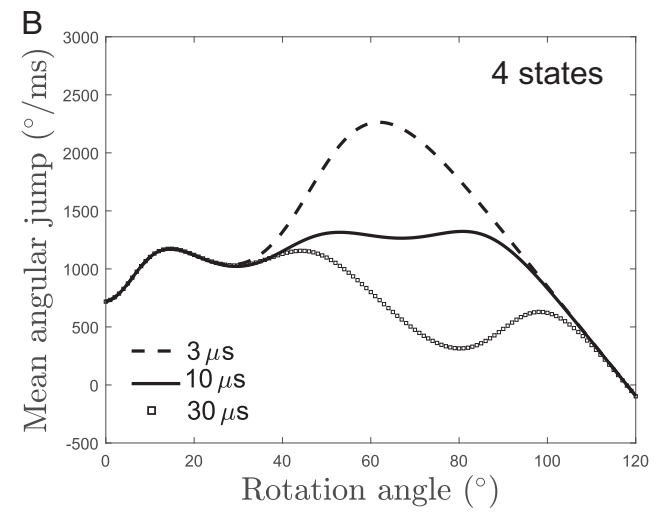


Fig. 5. (A) Theoretical predictions for the angular jump profile at 10 mM ATP concentration for 3- and 4-state model. (B) Theoretical angular jump profiles of 4-state model with different lifetimes of the metastable state (3, 10, and 30 μs).

Volkán-Kacsó et al. PNAS Latest Articles | 5 of 6

which is complementary to the stalling method, free rotation experiments are used that are 10^2 to 10^3 faster than stalling experiments.

3) ADP release is accelerated by 6 orders of magnitude by ATP binding. It has been suggested (31) that a 3-occupancy structure resolved by X-ray crystallography (25) may be similar to the metastable state during the ATP binding-assisted ADP release. The current analysis provides an estimate for the lifetime of 10 µs for this state. In contrast, the spontaneous ADP release takes tens of seconds (3). The lifetime of the triply occupied state then is some 6 orders of magnitude faster than that for ADP release from a singly occupied F₁-ATPase, so, in a concerted mechanism, the bottleneck due to a slow nucleotide release is eliminated, which is a necessary condition for a fast and efficient rotation cycle.

Materials and Methods

Theoretical Angular Jump Distribution and Average Jump. The θ -dependent angular jump distribution function $\rho(\Delta\theta|\theta)$ is calculated by solving Eq. 2 for the probability distribution $\rho_i(\theta, t)$, then averaging over the transition time T. We note that time averaging is also performed as part of extracting the distributions from the trajectories (SI Appendix), that is, by averaging over jumps that occur at various times during the many transitions in a trajectory that contains many 120° cycles. It yields the contributions $p_i(\theta)$ from state i, $p_i(\theta) = \int_0^T dt \rho_i(\theta, t) / \sum_i \int_0^T dt \rho_i(\theta, t)$. Then, a summation over all states yields $\rho(\Delta\theta/\Delta t|\theta)/\Delta t = \sum_{i} \rho_{ii}(\Delta\theta|\theta)p_{i}(\theta)$, where the probability distribution function $\rho(\Delta\theta/\Delta t|\theta)$ is normalized to unity with respect to variable $\Delta\theta/\Delta t$; that is, $\int \rho(\Delta\theta/\Delta t|\theta)d\Delta\theta/\Delta t=1$. We note that contributions to this sum from jumps during which there is a change in state (e.g., $i \rightarrow i+1$) have been neglected. The heta-dependent average angular jump $\langle \Delta \theta / \Delta t \rangle$ can be evaluated by expressing the expectation value of $\Delta \theta / \Delta t$ using Eq. 3 one component i at a time. It yields the θ -dependent mean, $\langle \Delta \theta \rangle = \sum_{i} (\theta_{i} - \theta) p_{i}(\theta) \Delta t / \tau.$

- 1. P. D. Boyer, The binding change mechanism for ATP synthase Some probabilities and possibilities. Biochim. Biophys. Acta 1140, 215-250 (1993).
- 2. J. P. Abrahams, A. G. W. Leslie, R. Lutter, J. E. Walker, Structure at 2.8 Å resolution of F₁-ATPase from bovine heart mitochondria. Nature 370, 621-628 (1994).
- K. Adachi et al., Coupling of rotation and catalysis in F₁-ATPase revealed by singlemolecule imaging and manipulation. Cell 130, 309-321 (2007).
- 4. S. Volkán-Kacsó, R. A. Marcus, What can be learned about the enzyme ATPase from single-molecule studies of its subunit F1? Quart. Rev. Biol. 50, e14 (2017).
- 5. H. Noji, R. Yasuda, M. Yoshida, K. Kinosita Jr, Direct observation of the rotation of F₁-ATPase. Nature 386, 299-302 (1997).
- 6. R. Yasuda, H. Noji, M. Yoshida, K. Kinosita Jr, H. Itoh, Resolution of distinct rotational substeps by submillisecond kinetic analysis of F1-ATPase. Nature 410, 898-904 (2001).
- 7. R. Watanabe, R. Iino, H. Noji, Phosphate release in F₁-ATPase catalytic cycle follows ADP release. Nat. Chem. Biol. 6, 814-820 (2010).
- 8. R. Watanabe, H. Noji, Timing of inorganic phosphate release modulates the catalytic activity of ATP-driven rotary motor protein. Nat. Commun. 5, 3486
- 9. C. B. Li, H. Ueno, R. Watanabe, H. Noji, T. Komatsuzaki, ATP hydrolysis assists phosphate release and promotes reaction ordering in F₁-ATPase. Nat. Commun. 6, 10223
- 10. D. Spetzler et al., Single molecule measurements of F₁-ATPase reveal an interdependence between the power stroke and the dwell duration. Biochem. 48, 7979-7985 (2009).
- 11. R. Watanabe et al., Mechanical modulation of catalytic power on F₁-ATPase, Nat. Chem. Biol. 8, 86-92 (2012).
- 12. K. Adachi, K. Oiwa, M. Yoshida, T. Nishizaka, K. Kinosita Jr. Controlled rotation of the F₁-ATPase reveals differential and continuous binding changes for ATP synthesis. Nat. Commun. 3, 1022 (2012).
- 13. R. Watanabe, K. Hayashi, H. Ueno, H. Noji, Catalysis-enhancement via rotary fluctuation of F₁-ATPase. Biophys. J. 105, 2385-2391 (2013).
- 14. W. Junge, H. Sielaff, S. Engelbrecht, Torque generation and elastic power transmission in the rotary FOF1-ATPase. Nature 459, 364-370 (2009).
- S. Volkán-Kacsó, R. A. Marcus, Theory of controlled rotation experiments, predictions, tests and comparison with stalling experiments in F1-atpase. Proc. Natl. Acad. Sci. U.S.A. 113, 12029-12034 (2016).
- 16. H. Risken, The Fokker-Planck Equation (Springer, Berlin, Germany, 2nd extended ed.,
- 17. G. Oster, H. Wang, Reverse engineering a protein: The mechanochemistry of ATP synthase. Biochim. Biophys. Acta 1458, 482-510 (2000).

Average Jump and the Relaxation Time. If the system is in a particular state i, for arbitrary time step Δt , the distribution in Eq. 3 is a Gaussian (as in equation 5.28 in ref. 16) that has a peak and a mean at $\langle \Delta \theta \rangle = -(\theta - \theta_i)(1 - \theta_i)$ $e^{-\Delta t/\tau}$). In the $\Delta t \ll \tau$ limit, the mean $\langle \Delta \theta/\Delta t \rangle$ will yield the relaxation time as the inverse of the angular slope, $1/\tau = D\beta \kappa_r \approx -\partial \langle \Delta\theta/\Delta t \rangle/\partial\theta$. For a constant time step Δt , $\langle \Delta \theta / \Delta t \rangle = \langle \Delta \theta \rangle / \Delta t$, and so, in the most general case,

$$\tau = -\Delta t / \log \left[1 + \left(\partial \left\langle \Delta \theta \right\rangle / \partial \theta \right)^{-1} \right].$$
 [6]

Quantities Used in the 3-State Model. No adjustable parameters were used in the above 3-state model. The quantities used in the theoretical calculations and their sources are listed in Table 1. Using data in the catalytic dwell, au was estimated from the angle autocorrelation function (Fig. 3A, Inset), while the angle histograms yielded κ_r (SI Appendix, Fig. S9). D was then calculated using Eq. 1. Previously, κ_r was found to be the same in the binding and catalytic dwells (11), and so we used the same κ_r for both i = 2 and 3. If D is mainly due to the viscous load on the probe, its value is also expected to be the same for the different is. Stalling experiments (11) yielded the $k_{fi}(\theta)$ values. The reverse rate constants in the transition were assumed to be negligibly small: The Pi (re)binding time constant is in the millisecond range at 1 mM concentration (11), and the spontaneous release of ATP takes seconds to complete (12). We note that a reverse mechanism in which ADP rebinding would assist ATP release is unlikely to yield a significant ATP release rate, due to low ADP concentrations in the solution. Previous single-molecule rotation experiments (3) yielded the dwell angles.

Data Availability. Computer code (Matlab) for simulations and data analysis is available upon request from the authors.

ACKNOWLEDGMENTS. We thank Drs. Hiroshi Ueno and Hiroyuki Noji for sharing their single-molecule rotation data for use in this analysis. L.O.L. acknowledges the support from Ian Ferguson Postgraduate Fellowship for his stay at California Institute of Technology. This work was also supported by the Office of the Naval Research, the Army Research Office, the James W. Glanville Foundation, the Society of Interdisciplinary Research, and Hong Kong University of Science and Technology Grants IGN17SC04 and R9418.

- 18. S. Volkán-Kacsó, R. A. Marcus, Theory for rates, equilibrium constants, and Brønsted slopes in F₁-ATPase single molecule imaging experiments. Proc. Natl. Acad. Sci. U.S.A. 112, 14230-14235 (2015).
- 19. H. Sielaff et al., Power stroke angular velocity profiles of archaeal A-ATP synthase versus thermophilic and mesophilic F-ATP synthase molecular motors. J. Biol. Chem. 116, 745240 (2016).
- 20. T. Uchihashi, R. Jino, T. Ando, H. Noji, High-speed atomic force microscopy reveals rotary catalysis of rotorless F₁-ATPase. Science 333, 755-758 (2011).
- 21. S. Volkán-Kacsó, R. A. Marcus, Theory of long binding events in single-moleculecontrolled rotation experiments on F1-ATPase. Proc. Natl. Acad. Sci. U.S.A. 114, 7272-7277 (2017).
- 22. I. Gopich, A. Szabo, Theory of the statistics of kinetic transitions with application to single-molecule enzyme catalysis. J. Chem. Phys. 124, 154712 (2006).
- 23. S. Volkán-Kacsó, Two-state theory of binned photon statistics for a large class of waiting time distributions and its application to quantum dot blinking. J. Chem. Phys. 140, 224110 (2014).
- 24. H. S. Chung et al., Extracting rate coefficients from single-molecule photon trajectories and FRET efficiency histograms for a fast-folding protein. J. Phys. Chem. A 115, 3642-3656 (2011).
- 25. R. Menz, J. E. Walker, A. G. Leslie, Structure of bovine mitochondrial F₁-ATPase with nucleotide bound to all three catalytic sites: Implications for the mechanism of rotary catalysis. Cell 106, 331-341 (2001).
- 26. J. L. Martin, R. Ishmukhametov, D. Spetzler, T. Hornung, W. D. Frasch, Elastic coupling power stroke mechanism of the F1-ATPase molecular motor. Proc. Natl. Acad. Sci. U.S.A. 115, 5750-5755 (2018).
- 27. K. Nam. M. Karplus. Insights into the origin of the high energy-conversion efficiency of F1-ATPase. Proc. Natl. Acad. Sci. U.S.A. 116, 15924-15929 (2019).
- 28. H. S. Chung, K. McHale, J. M. Louis, W. A. Eaton, Single-molecule fluorescence experiments determine protein folding transition path times. Science 335, 981-984 (2012).
- 29. P. Cossio, G. Hummer, A. Szabo, Transition paths in single-molecule force spectroscopy. J. Chem. Phys. 148, 123309 (2018).
- 30. E. Saita, T. Suzuki, K. Kinosita, M. Yoshida, Simple mechanism whereby the F₁-ATPase motor rotates with near-perfect chemomechanical energy conversion. Proc. Natl. Acad. Sci. U.S.A. 112, 9626–9631 (2015).
- 31. S. Mukherjee, A. Warshel, Electrostatic origin of the mechanochemical rotary mechanism and the catalytic dwell of F1-ATPase. Proc. Natl. Acad. Sci. U.S.A. 108, 20550-20555 (2011).
- T. Nishizaka et al., Chemomechanical coupling in F₁-ATPase revealed by simultaneous observation of nucleotide kinetics and rotation. Nat. Struct. Mol. Biol. 11, 142-148